Discrete Geodesic Regression in Shape Space

Benjamin Berkels[1], P. Thomas Fletcher[2], Behrend Heeren[1], Martin Rumpf[1], and Benedikt Wirth[3]

[1] Institute for Numerical Simulation, Universität Bonn
{benjamin.berkels,behrend.heeren,martin.rumpf}@ins.uni-bonn.de
[2] Scientific Computing and Imaging Institute, University of Utah
fletcher@sci.utah.edu
[3] Courant Institute of Mathematical Sciences, New York University
Benedikt.Wirth@cims.nyu.edu

Abstract. A new approach for the effective computation of geodesic regression curves in shape spaces is presented. Here, one asks for a geodesic curve on the shape manifold that minimizes a sum of dissimilarity measures between given two- or three-dimensional input shapes and corresponding shapes along the regression curve. The proposed method is based on a variational time discretization of geodesics. Curves in shape space are represented as deformations of suitable reference shapes, which renders the computation of a discrete geodesic as a PDE constrained optimization for a family of deformations. The PDE constraint is deduced from the discretization of the covariant derivative of the velocity in the tangential direction along a geodesic. Finite elements are used for the spatial discretization, and a hierarchical minimization strategy together with a Lagrangian multiplier type gradient descent scheme is implemented. The method is applied to the analysis of root growth in botany and the morphological changes of brain structures due to aging.

1 Introduction

Geodesic paths in shape space are the natural generalization of straight lines in Euclidian space. Applications include shape modeling in computer vision and graphics [1,2] or in computational anatomy [3,4], and shape clustering [5] as well as shape statistics [6]. As a generalization of linear regression in Euclidian space we investigate in this paper geodesic paths in shape space which best approximate given time indexed sets of input shapes in a least squares sense. Fig. 1 shows a discrete geodesic regression path in the space of 3D objects representing the growth process of sugar beet roots over a vegetation period.

Time-dependent shape statistics and shape regression has already been investigated in [7], where the regression curve is obtained via a simultaneous kernel weighted averaging in time and on shape space. In the application to brain images the kernel on shape space is linked to the Sobolev metric from the group of diffeomorphisms approach [8]. A variational formulation of geodesic regression is given in [9], where for given input shapes $\mathbf{S}_i$ at times t_i the (in a least squares sense) best approximating geodesic is computed as the minimizer of the energy

A. Heyden et al. (Eds.): EMMCVPR 2013, LNCS 8081, pp. 108–122, 2013.

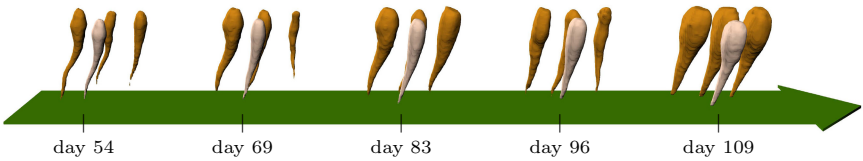

Fig. 1. Discrete regression curve (bright) for sugar beet input shapes (dark) at 5 different days in the vegetation period

$E[\mathbf{S}, v] = \frac{1}{2}\sum_i \mathrm{dist}^2(\exp_p(t_i\, v), \mathbf{S}_i)$ over the initial shape $\mathbf{S}$ of the geodesic path and its initial velocity or momentum v. Here, $\mathrm{dist}(\cdot,\cdot)$ is the Riemannian distance and exp the exponential map. A computationally efficient method in the group of diffeomorphisms shape space is based on duality calculus in constrained optimization and presented in [10]. In [11], a generalization allowing for image metamorphosis—simultaneous diffeomorphic image deformation and image intensity modulation—is proposed. In contrast to these approaches, we here do not minimize over the initial data of geodesic shooting but directly over the shapes along a time discrete geodesic. The classical energy minimization property of cubic splines exploited in the shape space context in [12] is related to the penalty used in our approach, which is defined via the L^2 integral of the covariant derivative of the shape velocity along shape curves.

There is a rich diversity of underlying Riemannian structures in the shape space context. On the space of planar curves the L^2-metric on direction and curvature functions is proposed in [1], and the L^2-metric on stretching and bending variations in [13], as well as curvature-weighted L^2- or Sobolev-type metrics in [14,15], some of which allow closed-form geodesics [16,17]. In the flow of diffeomorphism approach [18] the metric $g(v,v) = \int_D Lv \cdot v \,\mathrm{d}x$ is defined on Eulerian motion fields v for a higher order elliptic operator L on some computational domain $D \subset \mathbb{R}^d$. Fuchs et al. [19] propose a viscous-fluid based Riemannian metric related to the approach considered here. Here, we take up the time discrete concept proposed in [20] and define time discrete geodesics as minimizers of a time discrete path energy. In the concrete application, the path energy consists of a sum of matching energies, whose Hessian at the identity coincides with the rate of viscous dissipation generated by the shape deformation.

The paper is organized as follows. Based on a brief review in Section 2 of the concept of discrete geodesics proposed in [20] we develop a general variational model for shape regression in Section 3. In Section 4 this model is illustrated for the case of a finite dimensional manifold embedded in Euclidian space. Then, in Section 5 we investigate the application to the space of viscous fluidic objects. The algorithmic ingredients required to solve the underlying optimization problem are studied in detail in Section 6. The application of the method to shape statistics in anatomy and botany is presented in Section 7. Finally, in Section 8 we draw conclusions.

2 Discrete Geodesics in Shape Space

In this section, we briefly review the notion of continuous geodesics on shape spaces considered as Riemannian manifolds and adopt a recently introduced variational time discretization [20]. Let $\mathcal{M}$ denote the space of shapes as a Riemannian manifold with a metric $g_{\mathbf{S}}$ acting on variations $\dot{\mathbf{S}}$ of shapes $\mathbf{S}$ which are considered as tangent vectors on the manifold $\mathcal{M}$. A curve $\mathbf{S} : [0,1] \to \mathcal{M}$ with $\mathbf{S}(0) = \mathbf{S}_A$ and $\mathbf{S}(1) = \mathbf{S}_B$ is a geodesic if it is a local minimizer of the path energy $\mathcal{E}[(\mathbf{S}(t))_{t\in[0,1]}] = \int_0^1 g_{\mathbf{S}(t)}(\dot{\mathbf{S}}(t), \dot{\mathbf{S}}(t))\,\mathrm{d}t$. Such curves solve $\nabla_{\dot{\mathbf{S}}(t)}\dot{\mathbf{S}}(t) = 0$, where ∇ denotes the Levi-Civita connection, and in addition $g_{\mathbf{S}(t)}(\dot{\mathbf{S}}(t), \dot{\mathbf{S}}(t)) = \text{const}$. The associated distance $\mathrm{dist}(\mathbf{S}_A, \mathbf{S}_B)$ is the minimal path length $\mathcal{L}[(\mathbf{S}(t))_{t\in[0,1]}] = \int_0^1 (g_{\mathbf{S}(t)}(\dot{\mathbf{S}}(t), \dot{\mathbf{S}}(t)))^{\frac{1}{2}}\,\mathrm{d}t$ and minimizers of the energy also minimize the path length. If a continuous path $(\mathbf{S}(t))_{t\in[0,1]}$ is sampled at times $t_k = k\tau$ for $k = 0, \ldots, K$ and $\tau := \frac{1}{K}$, Jensen's inequality implies the estimate $\mathcal{E}[(\mathbf{S}(t))_{t\in[0,1]}] \geq \frac{1}{\tau}\sum_{k=1}^{K} \mathrm{dist}^2(\mathbf{S}_{k-1}, \mathbf{S}_k)$ with $\mathbf{S}_k = \mathbf{S}(t_k)$. Here, equality holds for geodesic paths due to the constant speed property of energy minimizing paths. This observation allows us to derive the fundamental notion of a discrete geodesic: Approximating the local squared Riemannian distance $\mathrm{dist}^2(\cdot,\cdot)$ by a functional $\mathbf{W} : \mathcal{M} \times \mathcal{M} \to \mathbb{R}, (\mathbf{S}_1, \mathbf{S}_2) \mapsto \mathbf{W}[\mathbf{S}_1, \mathbf{S}_2]$ in such a way that $\mathrm{dist}^2(\mathbf{S}, \tilde{\mathbf{S}}) = \mathbf{W}[\mathbf{S}, \tilde{\mathbf{S}}] + O(\mathrm{dist}^3(\mathbf{S}, \tilde{\mathbf{S}}))$, we are naturally led to the *discrete path energy* $\mathbf{E}$

$$\mathbf{E}[\mathcal{S}_K] = K \sum_{k=1}^{K} \mathbf{W}[\mathbf{S}_{k-1}, \mathbf{S}_k] \tag{1}$$

for discrete paths $\mathcal{S}_K = (\mathbf{S}_0, \ldots, \mathbf{S}_K)$. A *discrete geodesic* (of order K) is then defined as a minimizer of $\mathbf{E}[\mathcal{S}_K]$ for fixed end points $\mathbf{S}_0, \mathbf{S}_K$. In this discrete model $\mathbf{W}[\mathbf{S}, \tilde{\mathbf{S}}]$ can be interpreted as the cost required to deform the shape $\mathbf{S}$ into the shape $\tilde{\mathbf{S}}$. The required approximation property already implies $\mathbf{W}[\mathbf{S}, \mathbf{S}] = 0$ and that for the first and second variation of $\mathbf{W}$ with respect to the second shape we have $\partial_{\mathbf{S}_2}\mathbf{W}[\mathbf{S}, \mathbf{S}] = 0$ and $\frac{1}{2}\partial^2_{\mathbf{S}_2}\mathbf{W}[\mathbf{S}, \mathbf{S}] = g_{\mathbf{S}}$ for smooth g and $\mathbf{W}$ (cf. the exposition in [20]).

3 Derivation of the Discrete Regression Model

Based on the concept of discrete geodesics revisited in the last section, we are now in the position to derive our discrete shape regression model from a corresponding model of continuous geodesic regression. Let us consider sets of input shapes $\{\mathbf{S}_k^i\}_{i=1,\ldots,i_k}$ for $k = 0, \ldots, K$, which represent sets of statistical measurements at times $t_k \in [0,1]$ on the shape manifold $\mathcal{M}$. As a notational simplification let us suppose already here that all times t_k at which input shapes are given are multiples of the time step size $\tau = \frac{1}{K}$ of the discrete model to be introduced later. Indeed, this is no severe restriction because a generalization to discrete geodesics with non-constant time step sizes is straightforward (actually, a non-constant time step has been used in the computation underlying Fig. 1).

Now we ask for a geodesic curve $\mathcal{S} = (\mathbf{S}(t))_{t\in[0,1]}$ on $\mathcal{M}$ which minimizes a sum of dissimilarity measures between the input shapes $\mathbf{S}_k^i$ and the associated shapes $\mathbf{S}(t_k)$ on the geodesic curve. More precisely, we aim at minimizing

$$\mathcal{F}[\mathcal{S}] = \sum_{k=0}^{K} \sum_{i=1}^{i_k} \mathrm{diss}[\mathbf{S}(t_k), \mathbf{S}_k^i] \tag{2}$$

under the constraint that $\mathcal{S}$ is actually a geodesic, namely that $\nabla_{\dot{\mathbf{S}}(t)}\dot{\mathbf{S}}(t) = 0$. In analogy to the standard linear regression model in $\mathbb{R}^n$ the measure $\mathrm{diss}[\cdot,\cdot]$ might be the squared (geodesic) distance on $\mathcal{M}$ (cf. [9]) or another in general nonlinear measure of shape dissimilarity. Based on the above discussed approximation properties $\mathrm{diss}[\mathbf{S}(t_k), \mathbf{S}_k^i] = \mathbf{W}[\mathbf{S}(t_k), \mathbf{S}_k^i]$ is a natural choice.

Instead of enforcing the strict constraint that $\mathcal{S}$ is a geodesic, we might alternatively consider a penalty approach with

$$\mathcal{F}^\epsilon[\mathcal{S}] = \mathcal{F}[\mathcal{S}] + \frac{C}{\epsilon}\int_0^1 g_{\mathbf{S}(t)}(\nabla_{\dot{\mathbf{S}}(t)}\dot{\mathbf{S}}(t), \nabla_{\dot{\mathbf{S}}(t)}\dot{\mathbf{S}}(t))\,\mathrm{d}t \tag{3}$$

for a small penalty parameter ϵ. Obviously, on geodesic curves $\mathcal{S}$ the two energies $\mathcal{F}^\epsilon[\mathcal{S}]$ and $\mathcal{F}[\mathcal{S}]$ coincide. As a scaling factor C we choose $\mathcal{F}[\mathcal{S}^{\mathrm{ref}}]$, where $\mathcal{S}^{\mathrm{ref}}$ is a curve in shape space with $\mathbf{S}^{\mathrm{ref}}(t_k)$ being the shape mean of the input shapes at time t_k in the sense of [21], i. e. $\mathbf{S}^{\mathrm{ref}}(t_k) = \mathrm{argmin}_{\tilde{\mathbf{S}}} \sum_{i=1}^{i_k} \mathrm{diss}[\tilde{\mathbf{S}}, \mathbf{S}_k^i]$.

Let us now derive a discrete analog of the above continuous variational problem and specifically ask for a discrete geodesic regression curve. Now, we consider discrete curves $(\mathbf{S}_0, \ldots, \mathbf{S}_K)$ in shape space and assume (potentially after reindexing) that $\{\mathbf{S}_k^i\}_{i=1,\ldots,i_k}$ is the set of input shapes attached to the time $t_k = k\tau$. If $i_k = 0$ then the corresponding set is empty, and in what follows the associated sums over i are defined to be zero. With this notation at hand the discrete geodesic regression problem reads as follows:

Find a discrete path $\mathcal{S}_K = (\mathbf{S}_0, \ldots, \mathbf{S}_K)$ *such that* $\mathbf{F}[\mathcal{S}_K] = \sum_{k=0}^{K} \sum_{i=1}^{i_k} \mathrm{diss}[\mathbf{S}_k, \mathbf{S}_k^i]$ *is minimal under the constraint that* $\mathcal{S}_K$ *is a discrete geodesic, i. e.* $\mathcal{S}_K$ *minimizes* $\mathbf{E}[(\mathbf{S}_0, \ldots, \mathbf{S}_K)]$ *among all discrete paths with same end shapes* $\mathbf{S}_0$ *and* $\mathbf{S}_K$.

To derive a discrete penalty approach we take into account a suitable approximation of the integrand of the continuous penalty energy. Indeed, for g and $\mathbf{W}$ sufficienty smooth $g_{\mathbf{S}(t_k)}(\nabla_{\dot{\mathbf{S}}(t_k)}\dot{\mathbf{S}}(t_k), \nabla_{\dot{\mathbf{S}}(t_k)}\dot{\mathbf{S}}(t_k)) = 4K^4\mathbf{W}(\tilde{\mathbf{S}}_k, \mathbf{S}(t_k)) + O(K^{-2})$ for each $k = 1, \ldots, K-1$, where $\tilde{\mathbf{S}}_k$ is the middle shape of the discrete geodesic $(\mathbf{S}_{k-1} = \mathbf{S}(t_{k-1}), \tilde{\mathbf{S}}_k, \mathbf{S}_{k+1} = \mathbf{S}(t_{k+1}))$, i. e.

$$\tilde{\mathbf{S}}_k = \mathrm{argmin}_{\mathbf{S}}\left(\mathbf{W}[\mathbf{S}_{k-1}, \mathbf{S}] + \mathbf{W}[\mathbf{S}, \mathbf{S}_{k+1}]\right). \tag{4}$$

This is a straightforward consequence of the convergence theory presented in [22]. Then, writing $\tilde{\mathcal{S}}_K = (\tilde{\mathbf{S}}_1, \ldots, \tilde{\mathbf{S}}_{K-1})$ and using the simple quadrature $\int_0^1 f(t)\mathrm{d}t = K\sum_{k=1}^{K-1} f(t_k) + O(\tau)$ we obtain a discrete penalty approach

$$\mathbf{F}^\epsilon[\mathcal{S}_K] = \mathbf{H}^\epsilon[\mathcal{S}_K, \tilde{\mathcal{S}}_K] = \mathbf{F}[\mathcal{S}_K] + \frac{4CK^3}{\epsilon}\sum_{k=1}^{K-1} \mathbf{W}[\tilde{\mathbf{S}}_k, \mathbf{S}_k] \tag{5}$$

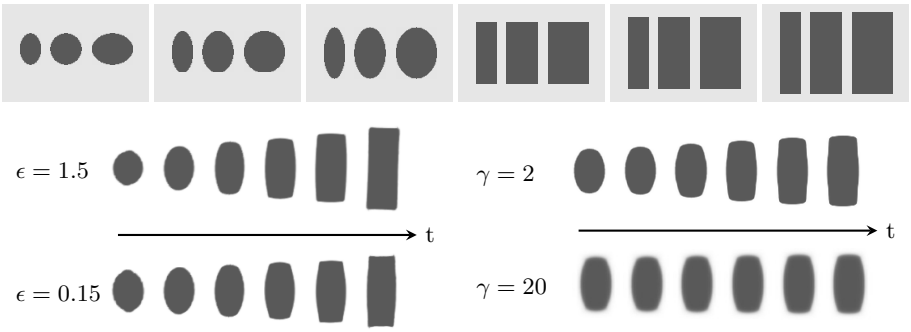

Fig. 2. Results of the discrete geodesic regression for given input objects at 6 timesteps (top row) are shown for different ϵ (left) and compared to the results obtained by using a simple path length penalty $\gamma\mathbf{E}[\mathcal{S}_K]$ (right)

and seek discrete paths which minimize this functional. The approach developed here is fairly general and will in Section 5 be applied to a concrete shape space, namely the space of viscous fluidic objects. Fig. 2 shows results of the discrete geodesic regression approach for different penalty parameters ϵ. For decreasing ϵ one observes an increased rounding effect towards the right of the curve, which reflects the global impact of the round input shapes on the resulting approximate discrete geodesic. These results are compared to regression curves obtained when replacing the proposed penalty by the simpler penalty $\gamma\,\mathbf{E}[\mathcal{S}_K]$, where $\mathbf{E}$ is the discrete path energy defined in (1). The latter leads to a collapse of the regression curve to a global shape average (cf. [21]).

4 Regression on a Finite Dimensional Manifold

At first, as a simple example and to further motivate our approach let us briefly demonstrate the discrete geodesic regression for the much simpler case of an m-dimensional surface $\mathcal{M}$ embedded in $\mathbb{R}^d$. We suppose $\mathcal{M}$ to be parametrized via a smooth parametrization $Y : \omega \to \mathbb{R}^d;\ \theta \mapsto Y(\theta)$ over a parameter domain ω. Furthermore, we consider the simple energy $\mathbf{W}[\tilde{\theta}, \theta] = |Y(\tilde{\theta}) - Y(\theta)|^2$, which reflects the stored elastic energy in a spring spanned between points $Y(\theta)$ and $Y(\tilde{\theta})$ through the ambient space of $\mathcal{M}$ in $\mathbb{R}^d$. Thus, the discrete path energy of a path $(\theta_0, \dots, \theta_K)$ is given by $\mathbf{E}[(\theta_0, \dots, \theta_K)] = K \sum_{k=1}^{K} |Y(\theta_k) - Y(\theta_{k-1})|^2$. Now, we suppose measurements θ_k^i to be given for $k = 0, \dots, K$, $i = 1, \dots, i_k$, i. e. $\{Y(\theta_k^i)\}_{i=1,\dots,i_k}$ are the corresponding input points on $\mathcal{M}$ at time $t_k = \tau k$. (As above $i_k = 0$ indicates an empty set of input points, and in what follows the associated sums over i are assumed empty.) Then the discrete regression problem reads as follows:

Find a discrete path $\Theta = (\theta_0, \dots, \theta_K)$ *and associated points* $\tilde{\Theta} = (\tilde{\theta}_1, \dots, \tilde{\theta}_{K-1})$ *such that* $\mathbf{H}^\epsilon[\Theta, \tilde{\Theta}] = \sum_{k=0}^{K} \sum_{i=1}^{i_k} |Y(\theta_k) - Y(\theta_k^i)|^2 + \frac{4K^3C}{\epsilon} \sum_{k=1}^{K-1} |Y(\tilde{\theta}_k) - Y(\theta_k)|^2$ *is minimal subject to the constraint that* $\tilde{\theta}_k$ *for* $k = 1, \dots, K-1$ *minimizes*

$\mathbf{G}(\theta_{k-1}, \theta, \theta_{k+1}) := |Y(\theta) - Y(\theta_{k-1})|^2 + |Y(\theta) - Y(\theta_{k+1})|^2$ *over all* $\theta \in \omega$.

Let us emphasize that the chosen parametrization influences the numerical solution process but not the resulting regression curves which solely depend on the manifold $\mathcal{M}$, the input data and the penalty parameter ϵ. Fig. 3 shows discrete regression curves on the sphere. In the implementation a parametrization via polar and azimuth angle was used. One clearly observes that for small ϵ the regression curve is close to a great circle so that sets of input points at a particular time might be located completely on one side of the regression curve. For larger values of ϵ the method still computes a smooth regression curve which better matches the input points at the expense of being far from a geodesic.

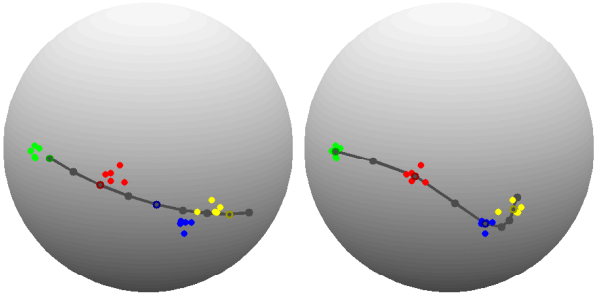

Fig. 3. Regression curve (black) for 20 input points on the unit sphere for a strong penalty weight with $\epsilon = 0.028$ (left) and just a mild curve smoothing with $\epsilon = 28$ (right)

The optimization algorithm. Denote by $\tilde{\Theta}[\Theta] = (\tilde{\theta}_1, \ldots, \tilde{\theta}_{K-1})$ the vector of minimizers of $\mathbf{G}(\theta_{k-1}, \cdot, \theta_{k+1})$, and define $\mathbf{F}^\epsilon[\Theta] = \mathbf{H}^\epsilon[\Theta, \tilde{\Theta}[\Theta]]$. The necessary condition for $\tilde{\theta}_k$ to minimize $\mathbf{G}(\theta_{k-1}, \cdot, \theta_{k+1})$ is $(2Y(\tilde{\theta}_k) - Y(\theta_{k-1}) - Y(\theta_{k+1}))^T DY(\tilde{\theta}_k) = 0$. To perform a gradient descent for the energy $\mathbf{F}^\epsilon$ we apply the duality techniques from constrained optimization [23] and define the dual solution $p_k \in \mathbb{R}^m$ as the solution of $D^2_\theta \mathbf{G}(\theta_{k-1}, \tilde{\theta}_k, \theta_{k+1}) p_k = \big(\partial_{\tilde{\theta}_k} \mathbf{H}^\epsilon\big)[\Theta, \tilde{\Theta}[\Theta]]$. Then we obtain $\partial_{\theta_k} \mathbf{F}^\epsilon[\Theta] = \big(\partial_{\theta_k} \mathbf{H}^\epsilon\big)[\Theta, \tilde{\Theta}(\Theta)] - \big(\partial_{\theta_k} \partial_{\tilde{\theta}_k} \mathbf{H}^\epsilon\big)[\Theta, \tilde{\Theta}[\Theta]]\, p_k$. The required derivatives of $\mathbf{G}$ and $\mathbf{H}^\epsilon$ are evaluated as follows,

$$D^2_\theta \mathbf{G}(\theta_{k-1}, \theta, \theta_{k+1})_{ij} = \sum_{n=1}^{d} \Big(2Y_{n,i}(\theta) Y_{n,j}(\theta) + (2Y_n(\theta) - Y_n(\theta_{k-1}) - Y_n(\theta_{k+1})) Y_{n,ij}(\theta) \Big) ,$$

$$\partial_{\tilde{\theta}_k} \mathbf{H}^\epsilon[\Theta, \tilde{\Theta}]_i = \frac{8CK^3}{\epsilon} \sum_{n=1}^{d} (Y(\tilde{\theta}_k) - Y(\theta_k))_n Y_{n,i}(\tilde{\theta}_k) ,$$

$$\partial_{\theta_k} \partial_{\tilde{\theta}_k} \mathbf{H}^\epsilon[\Theta, \tilde{\Theta}]_{ij} = -\frac{8CK^3}{\epsilon} \sum_{n=1}^{d} Y_{n,j}(\theta_k) Y_{n,i}(\tilde{\theta}_k) .$$

5 Shape Regression in the Space of Viscous Fluidic Objects

Now we apply the general approach of discrete geodesic regression to a physically motivated shape space of viscous fluidic objects with a metric induced by the

notion of viscous dissipation. Here, we assume that a viscous flow model at least captures some characteristics of the usually much more complex underlying processes such as e. g. plant growth. To this end, one considers objects $\mathbf{S}$ which are homeomorphic to a reference object $\hat{\mathbf{S}} \subset \mathbb{R}^d$ $(d = 2, 3)$. In general, one is not interested in point to point correspondences between two different objects but represents the actual shape $\mathbf{S}$ by an equivalence class of deformations $[\phi] = \{\tilde{\phi} \,|\, \tilde{\phi}(\hat{\mathbf{S}}) = \mathbf{S}\}$. A family $(\phi(t))_{t\in[0,1]}$ of such deformations is associated with an Eulerian velocity field $v(t) = \dot{\phi}(t) \circ \phi^{-1}(t)$, and shape variations are equivalence classes of such motion fields with $\tilde{v} \sim v$ if $\tilde{v} \cdot n = v \cdot n$ on $\partial\mathbf{S}$, where n is the outer normal on $\partial\mathbf{S}$. Now, a physically motivated metric on shape variations is given by the minimal rate of dissipation in a Newtonian fluid occupying $\mathbf{S}$ when its free boundary moves according to the shape variation,

$$g_{\mathbf{S}}(v, v) = \min_{\{\tilde{v} \,|\, \tilde{v}\cdot n = v\cdot n \text{ on } \partial\mathbf{S}\}} \int_{\mathbf{S}} \tfrac{\lambda}{2}(\mathrm{tr}\epsilon[\tilde{v}])^2 + \mu \mathrm{tr}(\epsilon[\tilde{v}]^2)\,\mathrm{d}x\,, \tag{6}$$

where $\lambda,\ \mu > 0$, $\epsilon[v] = \frac{1}{2}(\nabla v + \nabla v^T)$ ($\lambda = \mu = 1$ in the examples). In this context, a matching functional $\mathbf{W}$ to approximate the resulting squared Riemannian distance locally can be defined via the minimization of a deformation energy $\hat{\mathbf{W}}[\mathbf{S}, \phi] = \int_{\mathbf{S}} W(D\phi)\,\mathrm{d}x$ over all matching deformations ϕ with $\phi(\mathbf{S}) = \tilde{\mathbf{S}}$, i. e. $\mathbf{W}[\mathbf{S}, \tilde{\mathbf{S}}] = \min_{\phi(\mathbf{S})=\tilde{\mathbf{S}}} \hat{\mathbf{W}}[\mathbf{S}, \phi]$ for some particular deformation energy density W. There are primarily two options to choose a W which both ensure the requested consistency of the functional $\mathbf{W}$ and the metric g, i. e. $\frac{1}{2}D^2_\phi \hat{\mathbf{W}}[\mathbf{S}, \mathrm{id}] = g_{\mathbf{S}}$. One could consider a simple linearized model with

$$W^l(D\phi) = \tfrac{\lambda}{2}(\mathrm{tr}\epsilon[\phi - \mathrm{id}])^2 + \mu \mathrm{tr}(\epsilon[\phi - \mathrm{id}]^2)\,. \tag{7}$$

The advantage of W^l is that it is quadratic in ϕ so that the Euler–Lagrange equations for a functional composed of such energy densities will be linear. However, this is at the expense of the resulting energy being rigid body motion invariant only in an infinitesimal sense so that a relatively large number K of time steps is required in (1) to obtain an approximate frame indifference of discrete geodesic paths. Full rigid body motion invariance for large deformations can be guaranteed only for certain classes of nonlinear models $W = W^{nl}$. A specifically useful example is the energy density

$$W^{nl}(D\phi) = \frac{\mu}{2}\mathrm{tr}(D\phi^T D\phi) + \frac{\lambda}{4}\det(D\phi)^2 - \left(\mu + \frac{\lambda}{2}\right)\log\det D\phi - \frac{d\mu}{2} - \frac{\lambda}{4}\,. \tag{8}$$

We refer to [20] for further details on this approach.

In our application of discrete geodesic regression the computationally most demanding task is the continual computation of the shapes $\tilde{\mathbf{S}}_k$ for the penalty terms $\mathbf{W}[\tilde{\mathbf{S}}_k, \mathbf{S}_k]$. Therefore it turns out to be favorable to use W^l in the definition of the $\tilde{\mathbf{S}}_k$ and the penalty functional, i. e. we choose

$$\mathbf{W}[\mathbf{S}, \tilde{\mathbf{S}}] := \min_{\phi(\mathbf{S})=\tilde{\mathbf{S}}} \hat{\mathbf{W}}^l[\mathbf{S}, \phi] \quad \text{with} \quad \hat{\mathbf{W}}^l[\mathbf{S}, \phi] = \int_{\mathbf{S}} W^l(D\phi)\,\mathrm{d}x \tag{9}$$

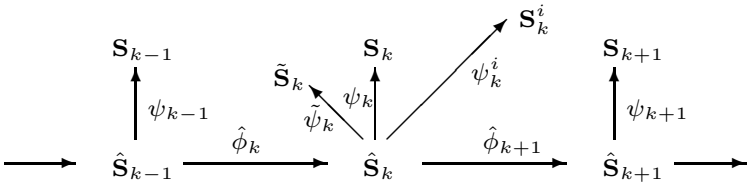

Fig. 4. A diagram illustrating the parametrization of the shapes $\mathbf{S}_k$ via deformations over reference shapes $\hat{\mathbf{S}}_k$. Here, $\hat{\phi}_k$ are given deformations such that $\hat{\mathbf{S}}_k = \hat{\phi}_k(\hat{\mathbf{S}}_{k-1})$.

in (4) and (5) and a large number of time steps K leading to a sufficiently small time step size $\tau = \frac{1}{K}$. The condition on $\tilde{\mathbf{S}}_k$ in (4) thus reads as

$$\tilde{\mathbf{S}}_k = \operatorname*{argmin}_{\mathbf{S}} \left(\min_{\phi(\mathbf{S}_{k-1})=\mathbf{S}} \hat{\mathbf{W}}^l[\mathbf{S}_{k-1}, \phi] + \min_{\phi(\mathbf{S})=\mathbf{S}_{k+1}} \hat{\mathbf{W}}^l[\mathbf{S}, \phi] \right) . \tag{10}$$

The treatment of the dissimilarity measure is computationally less critical and we would like to treat large scale variations between shapes of the discrete geodesic $\mathbf{S}_k$ and corresponding input shapes $\mathbf{S}_k^i$. Hence, here we take into account the nonlinear deformation model and define

$$\operatorname{diss}[\mathbf{S}_k, \mathbf{S}_k^i] := \min_{\phi(\mathbf{S}_k)=\mathbf{S}_k^i} \hat{\mathbf{W}}^{nl}[\mathbf{S}_k, \phi] \;\text{ with }\; \hat{\mathbf{W}}^{nl}[\mathbf{S}, \phi] = \int_{\mathbf{S}} W^{nl}(D\phi)\,\mathrm{d}x\,. \tag{11}$$

Finally, to render the method computationally feasible, we assume all deformations to be defined on a computational domain D ($D = [0,1]^d$ in the examples) containing all shapes under consideration, and we suppose that the material properties outside any of the shapes are by a factor δ softer than inside the shapes ($\delta = 0.01$ in the examples). Thus, we replace $\hat{\mathbf{W}}^{nl/l}[\mathbf{S}, \phi]$ by $\hat{\mathbf{W}}_\delta^{nl/l}[\mathbf{S}, \phi] := \int_D ((1-\delta)\chi_{\mathbf{S}} + \delta) W^{nl/l}(D\phi)\,\mathrm{d}x$ (where the superscript l or nl identifies the linear and the nonlinear model, respectively).

6 The Optimization Algorithm

Here we briefly describe the main algorithmic ingredients to minimize (5) in the context of the space of viscous fluidic objects. The presented variational approach for shape regression is based on functionals which depend on shapes and deformations defined on these shapes. To render the method computationally feasible, we parametrize shapes via deformations acting on reference shapes and work solely with deformations as unknowns. Then, we consider a gradient descent algorithm for the PDE constrained variational approach. In detail we proceed as follows:

Parametrizing shapes via deformations. The shapes $\mathbf{S}_k$ of the discrete geodesic as well as the constraint shapes $\tilde{\mathbf{S}}_k$ are represented via deformations ψ_k and $\tilde{\psi}_k$ of fixed reference shapes $\hat{\mathbf{S}}_k$, i. e. $\mathbf{S}_k = \psi_k(\hat{\mathbf{S}}_k)$ and $\tilde{\mathbf{S}}_k = \tilde{\psi}_k(\hat{\mathbf{S}}_k)$ (cf. Fig. 4). In addition, we consider deformations ψ_k^i on $\hat{\mathbf{S}}_k$ with $\mathbf{S}_k^i = \psi_k^i(\hat{\mathbf{S}}_k)$ for $i = 1, \ldots, i_k$.

We can now rephrase the deformations $\tilde{\phi}_k$ from the $\mathbf{S}_k$ onto the $\tilde{\mathbf{S}}_k$ (which occur in (5) via (9)) and the deformations $(\phi_k^i)_{k=1,\dots,K}^{i=1,\dots,i_k}$ from the shapes $\mathbf{S}_k$ onto the input shapes (which are introduced in (11) and used in $\mathbf{F}[\mathcal{S}_K]$) in terms of the above parametrizing deformations, i. e. $\phi_k^i = \psi_k^i \circ \psi_k^{-1}$, $\tilde{\phi}_k = \tilde{\psi}_k \circ \psi_k^{-1}$.

Approximation of the matching condition. To ensure that ϕ_k^i matches (at least approximately) $\mathbf{S}_k$ onto the input shape $\mathbf{S}_k^i$ we employ a penalty functional $P[\hat{\mathbf{S}}_k, \mathbf{S}_k^i, \psi_k^i] := \int_D |\chi_{\hat{\mathbf{S}}_k} - \chi_{\mathbf{S}_k^i} \circ \psi_k^i|^2 \,\mathrm{d}\hat{x}$ weighted with $\frac{C}{\eta}$ ($\eta = 0.1$ in the examples) and added to the total energy for all $k = 0, \dots, K$ and $i = 1, \dots, i_k$.

Expressing the energy in terms of the parametrizing deformations. To simplify notation, denote by $\Psi := (\psi_k, (\psi_k^i)_{i=1,\dots,i_k})_{k=0,\dots,K}$ the vector of all deformations which are considered as our actual degrees of freedom and by $\tilde{\Psi} := (\tilde{\psi}_1, \dots, \tilde{\psi}_{K-1})$ the vector of all constraint deformations. The energy $\mathbf{F}^\epsilon[\mathcal{S}_K]$ over which we minimize in (5) is rewritten as an energy $\hat{\mathbf{H}}^\epsilon_{\delta\eta}[\Psi, \tilde{\Psi}]$ of Ψ and $\tilde{\Psi}$,

$$\begin{aligned}\hat{\mathbf{H}}^\epsilon_{\delta\eta}[\Psi, \tilde{\Psi}] = &\sum_{k=0}^{K} \left(\sum_{i=1}^{i_k} \left(\hat{\mathbf{W}}^{nl}_\delta[\psi_k(\hat{\mathbf{S}}_k), \psi_k^i \circ \psi_k^{-1}] + \frac{C}{\eta} \mathbf{P}[\hat{\mathbf{S}}_k, \mathbf{S}_k^i, \psi_k^i] \right) \right) \\ &+ \frac{4CK^3}{\epsilon} \sum_{k=1}^{K-1} \hat{\mathbf{W}}^l_\delta[\psi_k(\hat{\mathbf{S}}_k), \tilde{\psi}_k \circ \psi_k^{-1}] \,. \end{aligned} \tag{12}$$

By the transformation rule we obtain the following computationally more efficient reformulation of the involved deformation energies

$$\hat{\mathbf{W}}^{nl/l}_\delta[\psi_k(\hat{\mathbf{S}}_k), \psi \circ \psi_k^{-1}] = \int_D ((1-\delta)\chi_{\hat{\mathbf{S}}_k} + \delta) W^{nl/l}\big(D\psi (D\psi_k)^{-1}\big) \det D\psi_k \,\mathrm{d}\hat{x} \tag{13}$$

for $\psi = \psi_k^i$ or $\psi = \tilde{\psi}_k$, respectively.

Realization of the constraint. We aim at minimizing $\mathbf{H}^\epsilon_{\delta\eta}$ subject to constraint (10). I. e. for all $k = 1, \dots, K-1$ the components $\tilde{\psi}_k$ of the vector of deformations $\tilde{\Psi}$ describe the middle shape of a discrete 3-shape geodesic with end shapes $\mathbf{S}_{k-1} = \psi_{k-1}(\hat{\mathbf{S}}_{k-1})$ and $\mathbf{S}_{k+1} = \psi_{k+1}(\hat{\mathbf{S}}_{k+1})$. We now slightly modify this constraint by requiring $\tilde{\psi}_k$ to be the minimizer of $\hat{\mathbf{W}}^l_\delta[\psi_{k-1}(\hat{\mathbf{S}}_{k-1}), \psi \circ \hat{\phi}_k \circ \psi_{k-1}^{-1}] + \hat{\mathbf{W}}^l_\delta[\psi(\hat{\mathbf{S}}_k), \psi_{k+1} \circ \hat{\phi}_{k+1} \circ \psi^{-1}]$ over all deformations ψ, where $\hat{\phi}_k$ are given matching deformations between the reference shapes with $\hat{\mathbf{S}}_k = \hat{\phi}_k(\hat{\mathbf{S}}_{k-1})$ (cf. Fig. 4). This is not quite the same as (10), not just because of the additional regularization, but also since here the point-to-point correspondence $\psi_{k+1} \circ \hat{\phi}_{k+1} \circ \hat{\phi}_k \circ \psi_{k-1}^{-1}$ between $\mathbf{S}_{k-1}$ and $\mathbf{S}_{k+1}$ is imposed along the 3-shape geodesic, which was not the case originally. Nevertheless, in the limit for $K \to \infty$ and $\epsilon \to 0$ the discrete path experimentally converges to a continuous geodesic (cf. Fig. 6 and 9).

A computationally advantageous symmetrization of the constraint. To fully exploit the quadratic deformation energy in the context of the above-mentioned constraint it is advantageous to further replace $\hat{\mathbf{W}}^l_\delta[\psi(\hat{\mathbf{S}}_k), \psi_{k+1} \circ \hat{\phi}_{k+1} \circ \psi^{-1}]$ by

$$\hat{\mathbf{W}}_\delta^{-l}[\psi_{k+1}(\hat{\mathbf{S}}_{k+1}), \psi \circ \hat{\phi}_{k+1}^{-1} \circ \psi_{k+1}^{-1}]$$
$$= \int_D ((1-\delta)\chi_{\hat{\mathbf{S}}_k} + \delta) W^l(D\psi(D\hat{\phi}_{k+1})^{-1}(D\psi_{k+1})^{-1} \circ \hat{\phi}_{k+1}) \cdot \det D\hat{\phi}_{k+1}(\det D\psi_{k+1}) \circ \hat{\phi}_{k+1} \mathrm{d}\hat{x}$$

which is quadratic in ψ and in effect replaces the relaxation of the energy $\min_{\phi(\mathbf{S})=\mathbf{S}_{k+1}} \hat{\mathbf{W}}^l[\mathbf{S}, \phi]$ in (10) by the relaxation of a similar energy based on the inverse deformation $\min_{\phi(\mathbf{S})=\mathbf{S}_{k+1}} \hat{\mathbf{W}}^l[\mathbf{S}_{k+1}, \phi^{-1}]$. For our applications (e. g. Fig. 6) we experimentally validated that for this computationally motivated modification the resulting discrete curves converge towards discrete geodesics. Altogether we obtain the following variational definition,

$$\tilde{\psi}_k := \operatorname*{argmin}_{\psi} \mathbf{G}[\psi_{k-1}, \psi, \psi_{k+1}] \tag{14}$$

for all $k = 1, \ldots, K-1$, where

$$\mathbf{G}[\psi_{k-1}, \psi, \psi_{k+1}] := \hat{\mathbf{W}}_\delta^l[\psi_{k-1}(\hat{\mathbf{S}}_{k-1}), \psi \circ \hat{\phi}_k \circ \psi_{k-1}^{-1}] + \hat{\mathbf{W}}_\delta^{-l}[\psi_{k+1}(\hat{\mathbf{S}}_{k+1}), \psi \circ \hat{\phi}_{k+1}^{-1} \circ \psi_{k+1}^{-1}] + \nu \hat{\mathbf{W}}^l[D, \psi]\,.$$

Here, we added $\nu\hat{\mathbf{W}}^l[D, \psi]$ as regularizer with $\nu \sim 10^{-2}h$ to ensure that not only the compositions of deformations are regular but also the deformation ψ.

A gradient descent scheme. We apply a standard Fletcher–Reeves nonlinear conjugate gradient descent to the above minimization problem, which at each step requires evaluation of the functional $\hat{\mathbf{F}}_{\delta\eta}^\epsilon[\Psi] := \hat{\mathbf{H}}_{\delta\eta}^\epsilon[\Psi, \tilde{\Psi}[\Psi]]$ and its gradient. For the functional evaluation, the quadratic optimization problem (14) is solved for each $k = 1, \ldots, K-1$ by a preconditioned linear conjugate gradient iteration. Using the standard adjoint method in constrained optimization [23] as in Section 4 we obtain the Gâteaux derivative of $\hat{\mathbf{F}}_{\delta\eta}^\epsilon[\Psi]$ (which incorporates constraint (14)) as

$$\partial_{\psi_k} \hat{\mathbf{F}}_{\delta\eta}^\epsilon[\Psi] = \left(\partial_{\psi_k} \hat{\mathbf{H}}_{\delta\eta}^\epsilon\right)[\Psi, \tilde{\Psi}[\Psi]] - \left(\partial_{\psi_k}\partial_{\tilde{\psi}_k} \hat{\mathbf{H}}_{\delta\eta}^\epsilon\right)[\Psi, \tilde{\Psi}[\Psi]]\, p_k\,, \tag{15}$$

where p_k is defined as the solution of the dual problem

$$D_\psi^2 \mathbf{G}[\psi_{k-1}, \tilde{\psi}_k, \psi_{k+1}]\, p_k = \left(\partial_{\tilde{\psi}_k} \hat{\mathbf{H}}_{\delta\eta}^\epsilon\right)[\Psi, \tilde{\Psi}[\Psi]]\,. \tag{16}$$

Different from the nonlinear energy $\hat{\mathbf{W}}^{nl}$, which is strictly rigid body motion invariant, the quadratic energy $\hat{\mathbf{W}}^l$ is rigid body motion invariant solely in an infinitesimal sense. Thus, in the case of large shape variability in the input data it turned out to be appropriate to enforce the preservation of the center of mass, $\int_D ((1-\delta)\chi_{\hat{\mathbf{S}}} + \delta)\psi \,\mathrm{d}\hat{x} = 0$, and the preservation of the angular momentum, $\int_D ((1-\delta)\chi_{\hat{\mathbf{S}}} + \delta)\left(D\psi - D\psi^T\right) \mathrm{d}\hat{x} = 0$, assuming the input shapes are co-aligned with respect to the zero moment and the direction of the first moment. This is implemented as an additional set of linear constraints in the minimization in (14) and in the outer minimization with respect to the energy term $\mathbf{W}_\delta^{nl}[\hat{\mathbf{S}}_k, \psi_k]$. The latter is realized by a projective gradient descent

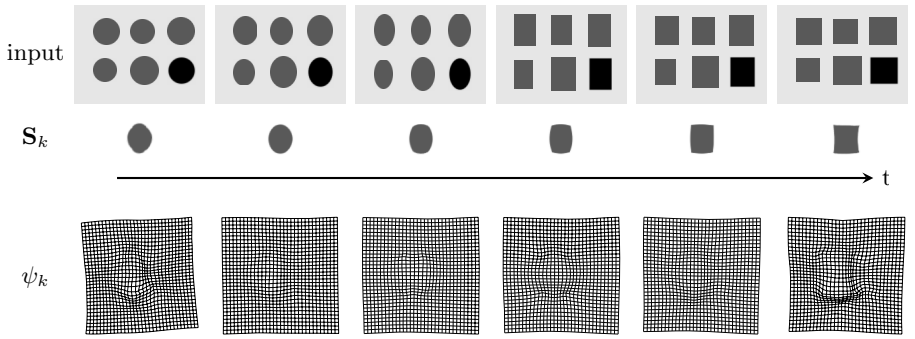

Fig. 5. Top: regression input shapes $(\mathbf{S}_k^i)_{k=0,\dots,5}^{i=1,\dots,5}$ (grey) and reference shapes $(\hat{\mathbf{S}}_k)_{k=0}^5$ (black), middle: discrete regression curve $(\mathbf{S}_k)_{k=0}^5$, bottom: the deformations $(\psi_k)_{k=0}^5$

scheme, the former by a Lagrange multiplier approach. To emphasize the qualitative behavior of geodesic regression we have computed the regression curve for a very basic test case. Fig. 5 displays a discrete geodesic and the associated deformations acting on the reference shapes, and Fig. 6 underlines that the resulting regression curves are actually very close to discrete geodesics. For the spatial discretization we employ multilinear finite elements on the computational domain $D = [0,1]^d$, which is overlaid with a regular square grid of $2^n + 1$, $n \in \mathbb{N}$, nodes in each direction. Energies are computed via Simpson quadrature on each element. Furthermore, we apply a cascadic approach, first computing the regression curve with a coarse spatial resolution for all involved deformations and then proceeding iteratively from coarse to fine. In this cascadic approach one can also adopt the reference shapes $\hat{\mathbf{S}}_k$ and the associated reference deformations $\hat{\phi}_k$ starting on the coarsest level with a single reference shape chosen as one of the coarsely resolved end shapes.

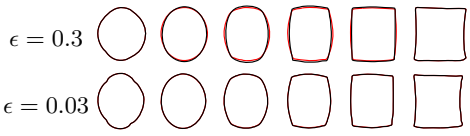

Fig. 6. Difference between the discrete regression curve (black) and the true discrete geodesic (red) connecting its end shapes for different ϵ.

7 Applications in Botany and Anatomy

We applied the geodesic regression approach to the statistical analysis of the aging of the human corpus callosum and to the growth of sugar beet roots over a vegetation period. Fig. 7 shows the discrete regression curve for the corpus callosum input shapes, which clearly reflects a substantial thinning of the structure with increasing age (cf. the results in [9] on a similar data set). Fig. 8 presents results obtained for 2D slices of sugar beet roots. Here, we also show the effect of an increasing number of intermediate shapes along the regression curve.

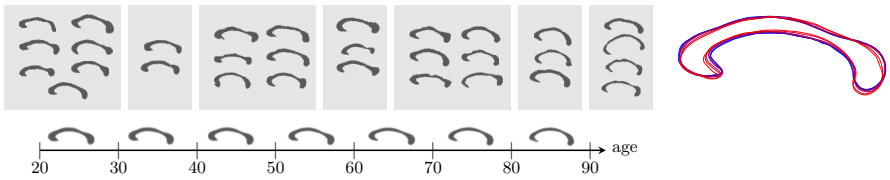

Fig. 7. Discrete geodesic regression curve for 31 shapes representing slices of the corpus callosum of humans at different age (2^{nd} to 8^{th} decade). On the right the 7 contours are overlayed showing a thinning process with increasing age (blue to red).

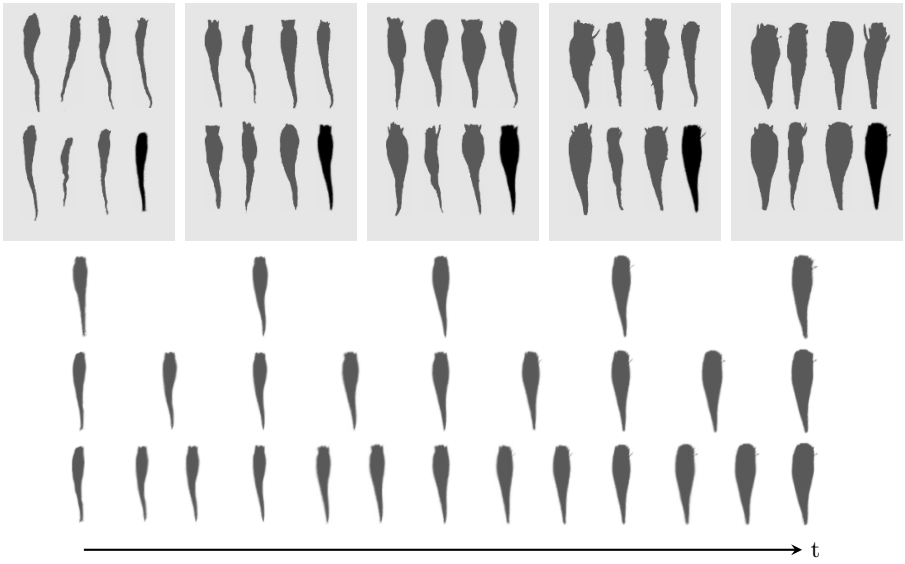

Fig. 8. From top to bottom: 2D input slices of sugar beets at five time points (grey) and shape averages for each time (black), regression curves for $\epsilon = 0.08$ and $K = 4, 8, 12$

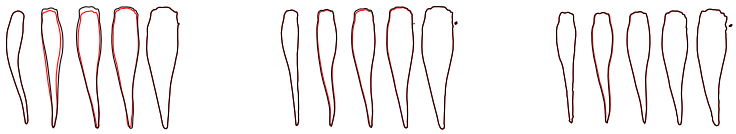

Fig. 9. Difference between the discrete regression curve (black) and the true discrete geodesic (red) connecting the end shapes for three different values of ϵ

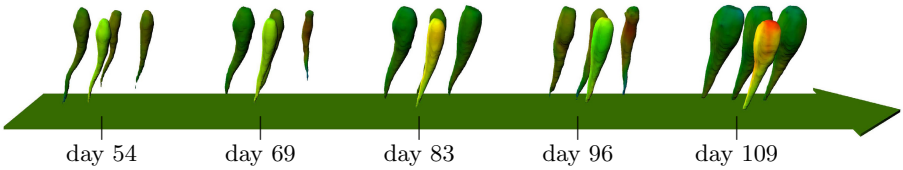

Fig. 10. For the discrete sugar beet regression curve (cf. Fig. 1) the shapes $\mathbf{S}_k$ in the front are color coded according to the signed distance from the shape average at each time point and the input shapes in the back according to the distance from the regression shape in front (colorcode: -0.127 — 0.061, maximal root height ≈ 0.75).

Fig. 9 once more demonstrates that already for moderately small penalty parameter ϵ the resulting curves are actually very close to a discrete geodesic. Finally, Fig. 10 shows some quantitative analysis of the regression curve for sugar beets in 3D.

8 Conclusions

We have described a time discrete geodesic regression approach on manifolds and applied it to the shape space of viscous fluidic objects. The method requires the solution of a PDE constrained optimization problem for deformations defined on a family of reference shapes. Applications in the context of plant growth and anatomical brain structures demonstrate the method's potential in time dependent shape statistics. A thorough convergence analysis for $K \to \infty$ and $\epsilon \to 0$ following the direction in [22] is still open. The current implementation based on a gradient descent approach requires several hours to compute a regression geodesic for 2D shapes and several days for 3D shapes. There is a great potential for faster energy relaxation using Newton type methods and more efficient parallel implementations. Furthermore, it would be interesting to investigate the generalization to more general classes of regression curves and the application to other shape spaces.

Acknowledgement. The 3D volumetric data of sugar beets acquired by 4.7T MRI are courtesy of R. Metzner (Forschungszentrum Jülich). The corpus callosum shape data was derived from MRI from the OASIS brain database (`www.oasis-brains.org`).

References

1. Klassen, E., Srivastava, A., Mio, W., Joshi, S.H.: Analysis of planar shapes using geodesic paths on shape spaces. IEEE Transactions on Pattern Analysis and Machine Intelligence 26(3), 372–383 (2004)
2. Kilian, M., Mitra, N.J., Pottmann, H.: Geometric modeling in shape space. ACM Transactions on Graphics 26, #64, 1–8 (2007)

3. Beg, M.F., Miller, M., Trouvé, A., Younes, L.: Computational anatomy: Computing metrics on anatomical shapes. In: Proceedings of 2002 IEEE ISBI, pp. 341–344 (2002)
4. Miller, M.I., Trouvé, A., Younes, L.: The metric spaces, Euler equations, and normal geodesic image motions of computational anatomy. In: Proceedings of the 2003 International Conference on Image Processing, vol. 2, pp. 635–638. IEEE (2003)
5. Srivastava, A., Klassen, E., Joshi, S.H., Jermyn, I.H.: Shape analysis of elastic curves in euclidean spaces. IEEE Transactions on Pattern Analysis and Machine Intelligence 33(7), 1415–1428 (2011)
6. Fletcher, P., Lu, C., Pizer, S., Joshi, S.: Principal geodesic analysis for the study of nonlinear statistics of shape. IEEE Transactions on Medical Imaging 23(8), 995–1005 (2004)
7. Davis, B., Fletcher, P.T., Bullitt, E., Joshi, S.: Population shape regression from random design data. In: Proceedings of IEEE International Conference on Computer Vision (2007)
8. Miller, M., Trouvé, A., Younes, L.: On the metrics and Euler-Lagrange equations of computational anatomy. Annual Review of Biomedical Enginieering 4, 375–405 (2002)
9. Fletcher, P.T.: Geodesic regression on Riemannian manifolds. In: MICCAI Workshop on Mathematical Foundations of Computational Anatomy (MFCA), pp. 75–86 (2011)
10. Niethammer, M., Huang, Y., Vialard, F.-X.: Geodesic regression for image time-series. In: Fichtinger, G., Martel, A., Peters, T. (eds.) MICCAI 2011, Part II. LNCS, vol. 6892, pp. 655–662. Springer, Heidelberg (2011)
11. Hong, Y., Joshi, S., Sanchez, M., Styner, M., Niethammer, M.: Metamorphic geodesic regression. In: Ayache, N., Delingette, H., Golland, P., Mori, K. (eds.) MICCAI 2012, Part III. LNCS, vol. 7512, pp. 197–205. Springer, Heidelberg (2012)
12. Trouvé, A., Vialard, F.X.: Shape splines and stochastic shape evolutions: a second order point of view. Quart. Appl. Math. 70(2), 219–251 (2012)
13. Srivastava, A., Jain, A., Joshi, S., Kaziska, D.: Statistical shape models using elastic-string representations. In: Narayanan, P.J., Nayar, S.K., Shum, H.-Y. (eds.) ACCV 2006. LNCS, vol. 3851, pp. 612–621. Springer, Heidelberg (2006)
14. Michor, P.W., Mumford, D.: Riemannian geometries on spaces of plane curves. J. Eur. Math. Soc. 8, 1–48 (2006)
15. Sundaramoorthi, G., Yezzi, A., Mennucci, A.: Sobolev active contours. International Journal of Computer Vision 73(3), 345–366 (2007)
16. Younes, L., Michor, P.W., Shah, J., Mumford, D.: A metric on shape space with explicit geodesics. Atti Accad. Naz. Lincei Cl. Sci. Fis. Mat. Natur. Rend. Lincei (9) Mat. Appl. 19(1), 25–57 (2008)
17. Sundaramoorthi, G., Mennucci, A., Soatto, S., Yezzi, A.: A new geometric metric in the space of curves, and applications to tracking deforming objects by prediction and filtering. SIAM Journal on Imaging Sciences 4(1), 109–145 (2011)
18. Dupuis, D., Grenander, U., Miller, M.: Variational problems on flows of diffeomorphisms for image matching. Quarterly of Applied Mathematics 56, 587–600 (1998)
19. Fuchs, M., Jüttler, B., Scherzer, O., Yang, H.: Shape metrics based on elastic deformations. J. Math. Imaging Vis. 35(1), 86–102 (2009)

20. Wirth, B., Bar, L., Rumpf, M., Sapiro, G.: A continuum mechanical approach to geodesics in shape space. International Journal of Computer Vision 93(3), 293–318 (2011)
21. Rumpf, M., Wirth, B.: A nonlinear elastic shape averaging approach. SIAM Journal on Imaging Sciences 2(3), 800–833 (2009)
22. Rumpf, M., Wirth, B.: Variational time discretization of geodesic calculus (2012), http://de.arxiv.org/abs/1210.2097
23. Fletcher, R.: Practical Methods of Optimization, 2nd edn. John Wiley & Sons (1987)